PHYSICAL REVIEW B VOLUME 27, NUMBER 6 15 MARCH 1983

Raman scattering study of the magnetic excitations in diluted magnetic semiconductors in the presence of an external magnetic field

A. Petrou, D. L. Peterson, S. Venugopalan,* R. R. Galazka,† A. K. Ramdas, and S. Rodriguez
Department of Physics, Purdue University, West Lafayette, Indiana 47907
(Received 14 October 1982)

We report the observation of Raman scattering associated with the magnetic excitations in diluted magnetic semiconductors, $Cd_{1-x}Mn_xTe$ in particular, in an applied magnetic field. A sharp Raman line due to the spin flip of the $3d$ electrons of Mn^{2+}, corresponding to the $\Delta m_S = \pm 1$ transition, occurs in the paramagnetic phase. Close to band-gap resonance, the $\Delta m_S = \pm 1$ transition in combination with the zone-center LO phonons as well as the $\Delta m_S = \pm 2$ transition are present. In addition to the internal transitions of Mn^{2+}, this resonance suggests a new Raman mechanism involving interband transitions in conjunction with the exchange interaction between band electrons and Mn^{2+}. In the magnetically ordered low-temperature phase, the magnon feature splits into two components in the presence of an applied magnetic field. As the temperature is lowered and the crystal becomes magnetically ordered, the Mn^{2+} spin flip of the paramagnetic phase evolves into the higher-energy component of the magnon.

I. INTRODUCTION

In a diluted magnetic semiconductor[1]—i.e., an alloy of a II-VI semiconductor with MnS, MnSe, or MnTe—the transition-metal ion substitutes for the group II element in a random fashion, e.g., in $Cd_{1-x}Mn_xTe$, Mn^{2+} replaces Cd^{2+}. The half-filled $3d$ shell of Mn has a spin $S=\frac{5}{2}$ and, hence the ion has a magnetic moment of 5.92 Bohr magnetons (μ_B). The exchange interaction between Mn^{2+} ions themselves, as well as that between Mn^{2+} ions and band electrons, underlies the unique magnetic behavior of the diluted magnetic semiconductors.[2] These alloys exhibit magnetic ordering at low temperatures[3–6] provided the magnetic ion concentration exceeds a minimum value characteristic of the alloy. Raman scattering from the magnetic excitations of the low-temperature magnetically ordered phases in $Cd_{1-x}Mn_xTe$ has recently been observed.[7,8] In this paper we report the effect of an external magnetic field on the magnetic excitations of diluted magnetic semiconductors in the different magnetic phases.[9]

II. EXPERIMENTAL PROCEDURE

The $Cd_{1-x}Mn_xTe$ crystals studied during the investigation were grown by a modified Bridgman method. The manganese concentration (x) of the samples was established by density and optical-absorption measurements; the range of composition was $0.0 < x < 0.70$. For $x > 0.70$, an inhomogeneous mixture of different compositions and crystallographic phases is obtained, and hence such crystals are unsuitable for these experiments. X-ray analysis showed that most of these samples are single crystals of the zinc-blende structure with the point group T_d. Some of the crystals, particularly those of higher concentration, showed a hexagonal symmetry when examined by the Laue method. However, the powder-diffraction method revealed that these samples have cubic symmetry. From these observations we concluded that these crystals are twinned.

In this paper our focus is mainly on $Cd_{1-x}Mn_xTe$, though preliminary experiments have been performed on the diluted magnetic semiconductors $Zn_{1-x}Mn_xTe$, $Cd_{1-x}Mn_xSe$, and $Cd_{1-x}Mn_xS$. $Zn_{1-x}Mn_xTe$ also has the zinc-blende structure, while $Cd_{1-x}Mn_xSe$ and $Cd_{1-x}Mn_xS$ have the wurtzite structure. The range of composition for $Zn_{1-x}Mn_xTe$ was $0.0 < x < 0.70$, for $Cd_{1-x}Mn_xSe$ it was $0.0 < x < 0.50$, and the $Cd_{1-x}Mn_xS$ crystal had a manganese concentration of $1M\,\%$.

The samples were oriented using the Laue method and optically polished according to the following procedure. The surfaces were ground in succession with 600-, 1200-, and 3200-grit carborundum powder. The initial polish was done on nylon cloth using 6-μm diamond paste. The final polish was done on microcloth saturated with a suspension of

 ©1983 The American Physical Society

0.05μm alumina powder in distilled water.

The Raman spectra were excited using the 7993-, 7525-, 6764-, 6471-, or 5682-Å line of a Kr^+-ion laser, the 6328-Å line of a He-Ne laser, or radiation from a dye laser, with Rhodamine-590 dye, pumped by an Ar^+-ion laser. The scattered light was analyzed using a double (triple) monochromator and detected using a standard photon counting system. As needed, the triple monochromator was used to reduce stray light, enabling us to observe weak Raman features to within 3 cm^{-1} of the exciting laser line.

The samples were inserted in an optical magnet cryostat[10] equipped with a superconducting coil, which enabled us to apply external magnetic fields up to 60 kG. The sample temperature was measured using a calibrated carbon-glass resistor located on the copper sample holder, immediately above the sample. A temperature controller[11] provided a stabilized temperature over the range 5–300 K.

The light scattering experiments were performed using right-angle, forward, and backscattering geometries. In the right-angle geometry the external magnetic field $\vec{H}$ was applied along the direction of either the incident ($\hat{k}_i$) or the scattered ($\hat{k}_s$) beam. Figure 1(a) shows the right-angle geometry with $\vec{H}||\hat{k}_i$. In this geometry the incident beam passes through a Babinet-Soleil compensator, set to produce either left-handed ($\hat{\sigma}_+$) or right-handed ($\hat{\sigma}_-$) circularly polarized light, where $\hat{\sigma}_\pm=(1/\sqrt{2})(\hat{x}\pm i\hat{y})$ and the beam is traveling along $\hat{z}$. The scattered light is analyzed along the direction of the magnetic field ($\hat{z}$). This light scattering configuration will be referred to as ($\hat{\sigma}_\pm,\hat{z}$). Figure 1(b) shows the right-angle geometry with $\vec{H}||\hat{k}_s$. The incident light is polarized along the direction of the magnetic field ($\hat{z}$). The polarization of the scattered radiation is analyzed as either $\hat{\sigma}_+$ or $\hat{\sigma}_-$ using a quarter-wave plate in combination with a linear analyzer. The forward scattering geometry is shown in Fig. 1(c). The incident and scattered light propagate along the direction of the magnetic field ($\hat{z}$). The polarization of the incident beam is either $\hat{\sigma}_+$ or $\hat{\sigma}_-$, and the scattered light is analyzed as either $\hat{\sigma}_+$ or $\hat{\sigma}_-$. In all three geometries the axes have been chosen such that $\hat{z}$ is always parallel to the magnetic field $\vec{H}$.

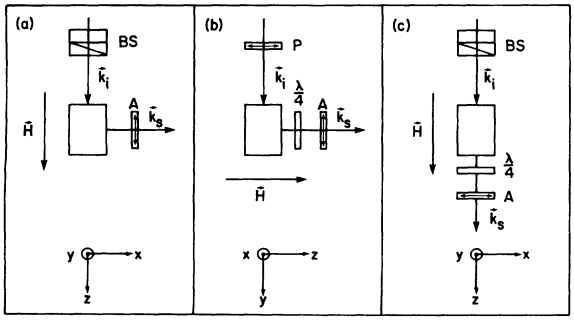

FIG. 1. Geometries for Raman scattering in the presence of a magnetic field with ($\hat{e}_i,\hat{e}_s$) polarization configuration, $\hat{e}_i$ being the incident and $\hat{e}_s$ the scattered polarization. The geometries in (a), (b), and (c) allow the ($\hat{\sigma}_\pm,\hat{z}$), ($\hat{z},\hat{\sigma}_\pm$), and ($\hat{\sigma}_\pm,\hat{\sigma}_\mp$) polarizations for the incident and scattered light, respectively. BS stands for the Babinet-Soleil compensator, *P* for the polarizer, *A* for an analyzer, and $\lambda/4$ for a quarter-wave plate. The axes are chosen such that $\hat{z}$ is parallel to $\vec{H}$.

III. EXPERIMENTAL RESULTS AND DISCUSSION

This paper discusses the magnetic excitations in diluted magnetic semiconductors. Since the focus is on $Cd_{1-x}Mn_xTe$, we shall describe briefly the magnetic phases of this material as determined by Galazka *et al.*[3] using specific-heat and magnetic susceptibility measurements. They have found that $Cd_{1-x}Mn_xTe$ crystals are paramagnetic at all temperatures for $x<0.17$. For compositions in the range $0.17<x<0.70$, the crystals are paramagnetic for high temperatures, and as the temperature is lowered a spin-glass is obtained for $0.17<x<0.60$, while for $0.60<x<0.70$, a paramagnetic to antiferromagnetic phase transition occurs.

A. Paramagnetic phase

In the paramagnetic phase the exchange interaction between Mn^{2+} ions is smaller than the thermal energy k_BT and the ions can be considered as being independent of one another. The $^6S_{5/2}$ ground state of the Mn^{2+} ion has a total spin $S=\frac{5}{2}$, orbital angular momentum $L=0$, and total angular momentum $J=\frac{5}{2}$. The cubic crystalline field (site symmetry T_d) splits the sixfold degenerate ground state into a Γ_8 quadruplet state at $+a$, and a Γ_7 doublet at $-2a$, where $3a$ is the crystal-field splitting.[12] From electron paramagnetic resonance (EPR) experiments, Lambe and Kikuchi[13] obtained $3a=0.0084$ cm^{-1} for Mn^{2+} in CdTe. This crystal-field splitting is too small to be observed with the resolution of our spectrometer, and, hence in our subsequent discussion we treat the ground state of Mn^{2+} in $Cd_{1-x}Mn_xTe$ as an atomic $^6S_{5/2}$ level. The application of an external magnetic field, $\vec{H}$, results in the removal of the sixfold degeneracy of the ground state, the energy levels being $E(m_S)=g\mu_BHm_S$. Here g is the Landé g factor of the Mn^{2+} ion, and m_S, the projection of $\vec{S}$ along $\vec{H}$, has the values $-\frac{5}{2}, -\frac{3}{2},\ldots,+\frac{5}{2}$. These energy levels form the Zeeman multiplet of the ground state of Mn^{2+}.

In the paramagnetic phase Raman scattering was used to observe the spin-flip transitions between adjacent sublevels of this multiplet. The results in $Cd_{1-x}Mn_xTe$ are shown in Fig. 2 for $x=0.40$. As can be seen, a strong Stokes and anti-Stokes line are observed with a Raman shift of $\omega_{PM}=5.62\pm0.02$ cm^{-1} at room temperature, where PM represents paramagnetic and with $H=60$ kG, the geometry being that of Fig. 1(a). The Stokes line is observed in the $(\hat{\sigma}_+,\hat{z})$ configuration, whereas the anti-Stokes line is seen in $(\hat{\sigma}_-,\hat{z})$. When the geometry of Fig. 1(b) is used, the Stokes component appears in the polarization $(\hat{z},\hat{\sigma}_-)$, while the anti-Stokes component is observed in $(\hat{z},\hat{\sigma}_+)$. Within experimental errors the frequency shift is linear in H. With the energy separation between adjacent sublevels of the Zeeman multiplet given by $\Delta E=g\mu_B H$, we find $g=2.01\pm0.02$. We have observed the Raman line at ω_{PM} in $Cd_{1-x}Mn_xTe$ for a variety of compositions ranging from $x=0.01$ to $x=0.70$. We have also observed it in $Zn_{1-x}Mn_xTe$, $Cd_{1-x}Mn_xSe$, and $Cd_{1-x}Mn_xS$. For a given temperature, the width of the ω_{PM} line is found to increase with Mn concentration, x. We draw attention to the EPR work of Oseroff *et al.*[14] and Oseroff,[15] which also showed this trend in the linewidths. It is reasonable to attribute this to the exchange interaction among Mn^{2+} ions, which is expected to be significant for increasing x and decreasing temperature. The above spin-flip transition, associated with the electrons localized on Mn^{2+} in the paramagnetic phase, is similar to that recently reported for Ce^{3+} in cerium magnesium nitrate.[16]

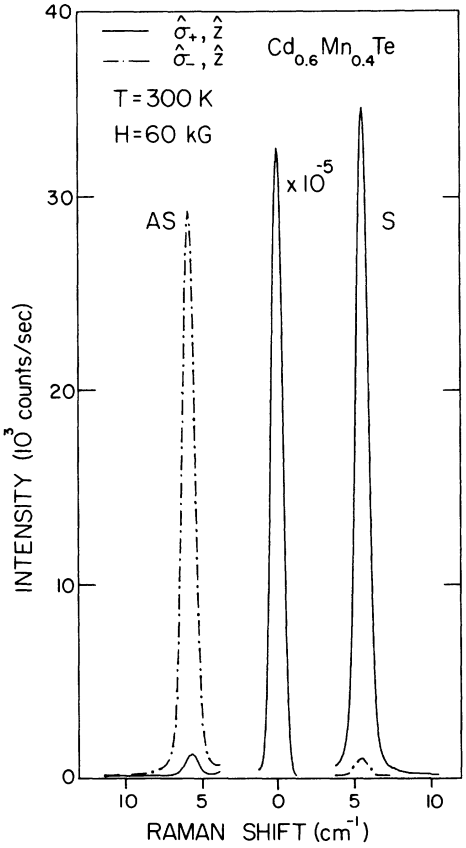

FIG. 2. Stokes (S) and anti-Stokes (AS) Raman lines at ω_{PM} resulting from $\Delta m_S=\pm1$ spin-flip transitions within the Zeeman multiplet of Mn^{2+} in $Cd_{1-x}Mn_xTe$, $x=0.40$. The wavelength of the exciting laser line $\lambda_L=6764$ Å; the applied magnetic field $H=60$ kG; x, y, and z are along [001], [1$\bar{1}$0], and [110], respectively.

Following the arguments given by Fleury and Loudon[17] one can consider, as a possible mechanism for the ω_{PM} Raman line, a two-step process having as the intermediate state one of the excited states of the Mn^{2+} ion ($L=1, S=\frac{5}{2}$). Figure 3 shows such mechanisms for the Stokes and anti-Stokes components of the ω_{PM} line. For the Stokes component an incident photon of energy $\hbar\omega_i$ and polarization $\hat{\sigma}_+$ induces a virtual electric dipole transition between an initial and an intermediate state which differ by $\Delta m_J=+1$; it is followed by a second electric dipole transition between the intermediate and final states with $\Delta m_J=0$. This is accompanied by the emission of a scattered photon of polarization $\hat{z}$ and energy $\hbar\omega_s=\hbar\omega_i-\hbar\omega_{PM}$. At the end of this process the Mn^{2+} ion is in an excited state within the Zeeman multiplet differing from the initial state by $\Delta m_S=+1$. The appearance of the Stokes component in the $(\hat{z},\hat{\sigma}_-)$ configuration is also illustrated in Fig. 3. Similar processes can be visualized for the anti-Stokes component having the $(\hat{\sigma}_-,\hat{z})$ or the $(\hat{z},\hat{\sigma}_+)$ polarization. This mechanism correctly predicts the experimentally observed polarization characteristics of the Stokes and anti-Stokes components of the ω_{PM} Raman line. We note that the selection rules are immediate consequences of conservation of angular momentum of the system

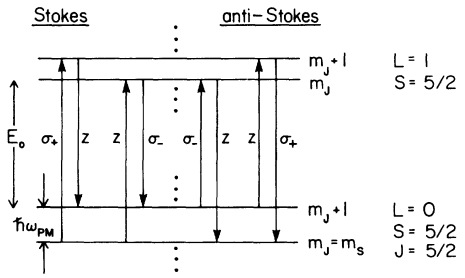

FIG. 3. Raman mechanism for the ω_{PM} line involving the internal transitions of the Mn^{2+} ion. The arrows indicate virtual electric dipole transitions. The energy level scheme is not to scale and the energy difference between the excited and ground states E_0 is much greater than $\hbar\omega_{PM}$.

comprised of the Mn^{2+} ions and the photon field. It should also be pointed out that the Stokes scattering process in the $(\hat{\sigma}_+,\hat{z})$ configuration is the time-reversed conjugate of the $(\hat{z},\hat{\sigma}_+)$ anti-Stokes process[18]; in the same manner, the $(\hat{z},\hat{\sigma}_-)$ Stokes and the $(\hat{\sigma}_-,\hat{z})$ anti-Stokes processes are related by time reversal.

The band gap of $Cd_{1-x}Mn_xTe$ has been observed to increase linearly with manganese concentration.[19] Exploiting the variation of the band gap with manganese concentration and/or temperature, we were able to match the band gap of several samples with the energy of one of the discrete lines of the Kr^+ laser. In addition, the dye laser was also used to achieve resonant conditions. We found that the intensity of the ω_{PM} line increased by several orders of magnitude as the laser photon energy approached that of the band gap. For instance, its intensity for $Cd_{1-x}Mn_xTe$ with $x=0.4$, recorded under identical conditions, varies from 15 counts per second (cps) for a laser wavelength of 7993 Å to 22 300 cps for 5908 Å.

Our observation of this resonant enhancement in the intensity of the ω_{PM} Raman line prompted the consideration of a mechanism involving interband transitions. This mechanism involves the Mn^{2+}-band electron exchange interaction which is described by the Hamiltonian[20]

$$H_x=\sum_n J(\vec{r}-\vec{R}_n)\vec{S}_n\cdot\vec{S}_e\ , \tag{1}$$

where J is the exchange integral, $\vec{r}$ and $\vec{S}_e$ are the position and spin operators of a band electron, and $\vec{S}_n$ and $\vec{R}_n$ are the spin operator and position for a Mn^{2+} ion. The term $\vec{S}_n\cdot\vec{S}_e$ can be written as

$$\vec{S}_n\cdot\vec{S}_e=S_n^zS_e^z+\tfrac{1}{2}S_n^+S_e^-+\tfrac{1}{2}S_n^-S_e^+\ . \tag{2}$$

Here $S_n^\pm$ and $S_e^\pm$ are the spin raising and lowering operators for a Mn^{2+} ion and band electron, respectively, and S_n^z and S_e^z are the corresponding projections of spin along $\hat{z}$. The second term of Eq. (2) raises the spin of a Mn^{2+} ion while simultaneously lowering the spin of a band electron, i.e.,

$$|m_S\rangle_{Mn^{2+}}|m_J\rangle_e\rightarrow|m_S+1\rangle_{Mn^{2+}}|m_J-1\rangle_e\ . \tag{3}$$

In a similar fashion, the third term lowers the spin of an ion while raising the spin of a band electron, i.e.,

$$|m_S\rangle_{Mn^{2+}}|m_J\rangle_e\rightarrow|m_S-1\rangle_{Mn^{2+}}|m_J+1\rangle_e\ . \tag{4}$$

Hence these terms can induce simultaneous changes in the spin states (simultaneous spin flips) of the band electrons on the one hand, and the Mn^{2+} ions on the other, corresponding to $\Delta m_S(Mn^{2+})=\pm1$ and $\Delta m_J(e)=\mp1$.

In Fig. 4 we show the above-mentioned mechanism for both the Stokes and the anti-Stokes component and the two right-angle geometries of Figs. 1(a) and 1(b). In the presence of a magnetic field the Γ_8 valence band splits into four subbands with $m_J=-\frac{3}{2}$, $-\frac{1}{2}$, $+\frac{1}{2}$, and $+\frac{3}{2}$, and the Γ_6 conduction band splits into $m_J=+\frac{1}{2}$ and $-\frac{1}{2}$ subbands. The possible processes for the Stokes component appearing in the $(\hat{\sigma}_+,\hat{z})$ configuration are shown in Fig. 4(a). In the first process, an incident photon of polarization $\hat{\sigma}_+$ is absorbed, raising an electron to the conduction band with $\Delta m_J=+1$ and creating a hole in the valence band. In the second step, the excited electron interacts with a Mn^{2+} ion via the second term of Eq. (2), resulting in $\Delta m_S(Mn^{2+})=+1$ and $\Delta m_J(e)=-1$. Finally, the electron and hole recombine emitting a photon of energy $\hbar\omega_s=\hbar\omega_i-\hbar\omega_{PM}$ of polarization $\hat{z}$; the band electrons have thus returned to their ground state, but leaving the Mn^{2+} ion excited to the next sublevel of the Zeeman multiplet. In the other two processes shown in Fig. 4(a), the hole, rather than the excited electron, interacts with the Mn^{2+} ion, resulting, however, in identical polarization selection rules. In the same manner, the Stokes component in the $(\hat{z},\hat{\sigma}_-)$ configuration follows from Fig. 4(c). The anti-Stokes processes for the $(\hat{\sigma}_-,\hat{z})$ and the $(\hat{z},\hat{\sigma}_+)$ geometries are shown in Figs. 4(b) and 4(d), respectively.

In the spirit of the above discussion one can also visualize a mechanism in which the Mn^{2+}-electron and Mn^{2+}-hole exchange interactions result in a similar Raman line but with a shift of $2\omega_{PM}$. The processes resulting in a Raman shift of $2\omega_{PM}$ are shown in Fig. 5. For example, in Fig. 5(a), a photon of polarization $\hat{\sigma}_+$ is absorbed, virtually exciting an electron from the $m_J=-\frac{1}{2}$ valence subband to the $m_J=+\frac{1}{2}$ conduction subband. The excited electron then interacts with a Mn^{2+} ion resulting in $\Delta m_S(Mn^{2+})=+1$ and $\Delta m_J(e)=-1$, while the hole in the valence band interacts in the same manner yielding $\Delta m_S(Mn^{2+})=+1$ and $\Delta m_J(e)=-1$. Figures 5(b) and 5(c) show how a Stokes shift of $2\omega_{PM}$ might arise exclusively through a Mn^{2+}-valence electron exchange interaction; from Eqs. (1) and (2) it is clear that such an interaction will involve two successive Mn^{2+} spin flips. Owing to the extended wave functions of both the conduction electron and the hole it should be more probable that this process involves two Mn^{2+} ions rather than just one. Similarly, the anti-Stokes components of the mechanism are those presented in Figs. 5(d)–5(f). Energy conservation requires that the energy of the scattered

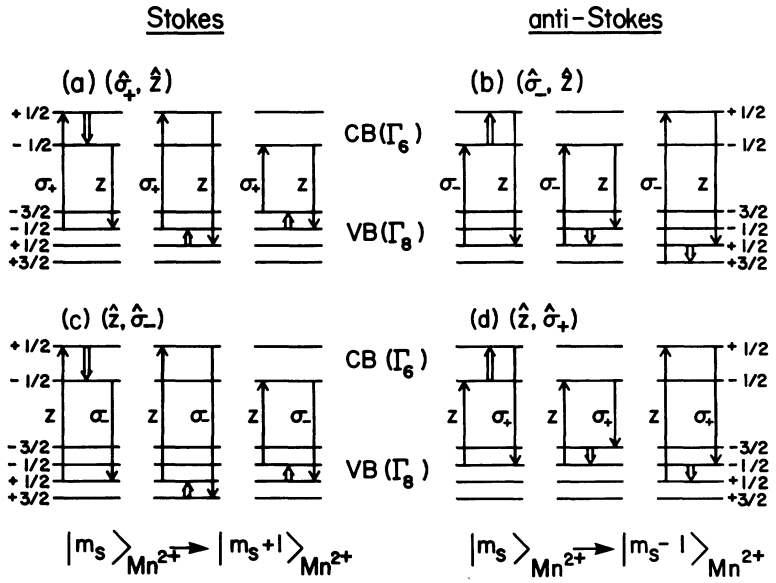

FIG. 4. Raman mechanism for the ω_{PM} line involving the band electrons. CB and VB refer to the conduction and valence bands, respectively, which are labeled by the electronic quantum number m_J. The single arrows indicate virtual electric dipole transitions, while the double arrows refer to transitions induced by the electron-Mn^{2+} exchange interaction. The allowed polarizations for the Stokes component are $(\hat{\sigma}_+,\hat{z})$ and $(\hat{z},\hat{\sigma}_-)$, while those for the anti-Stokes are $(\hat{\sigma}_-,\hat{z})$ and $(\hat{z},\hat{\sigma}_+)$.

photon be $\hbar\omega_s=\hbar\omega_i-2\hbar\omega_{PM}$. The polarization selection rules predicted by this mechanism are $(\hat{\sigma}_+,\hat{\sigma}_-)$ for the Stokes and $(\hat{\sigma}_-,\hat{\sigma}_+)$ for the anti-Stokes components of the Raman line at $2\omega_{PM}$. This mechanism is expected to be significant only close to resonance.

The Raman line at $2\omega_{PM}$ has been observed under resonant conditions for a variety of compositions. The results for $Cd_{1-x}Mn_xTe$ with $x=0.10$ are shown in Fig. 6; in this case, resonant conditions were achieved by maintaining a sample temperature of 120 K and using the 7525-Å line of the Kr^+ laser as the exciting radiation. The forward scattering geometry shown in Fig. 1(c) was used in order to ob-

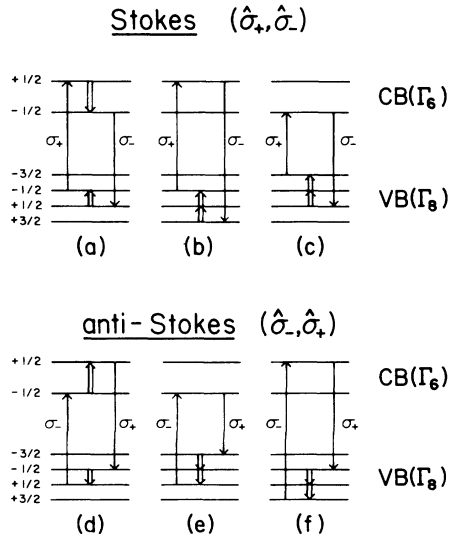

FIG. 5. Raman mechanism for the $\Delta m_S=\pm 2$ spin-flip transition, i.e., the $2\omega_{PM}$ line, involving the band electrons. The Stokes line is allowed in $(\hat{\sigma}_+,\hat{\sigma}_-)$ polarization, whereas the anti-Stokes appears in $(\hat{\sigma}_-,\hat{\sigma}_+)$.

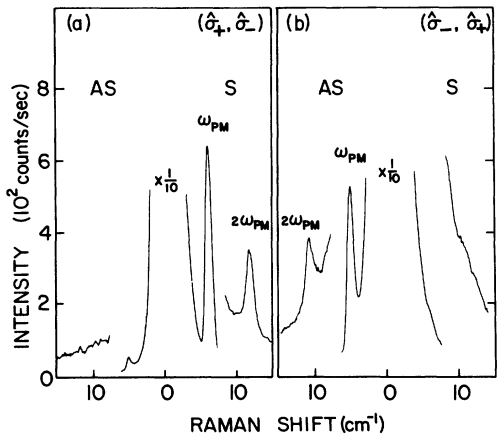

FIG. 6. Stokes and anti-Stokes components of $2\omega_{PM}$ in $Cd_{1-x}Mn_xTe$, $x=0.10$, recorded for the $(\hat{\sigma}_+,\hat{\sigma}_-)$ and $(\hat{\sigma}_-,\hat{\sigma}_+)$ polarizations using the geometry of Fig. 1(c). The sample temperature $T=120$ K, $H=60$ kG, and $\lambda_L=7525$ Å; x, y, and z are along [110], [$\bar{1}$10], and [001], respectively. The ω_{PM} line appearing in the spectra is due to leakage.

tain the $(\hat{\sigma}_+,\hat{\sigma}_-)$ and $(\hat{\sigma}_-,\hat{\sigma}_+)$ configurations. As can be seen in Fig. 6, the Stokes and the anti-Stokes lines appear with the expected polarizations. Under the resonant conditions of this experiment the ω_{PM} line is extremely intense ($\sim 10^6$ cps); although this line is forbidden for these polarizations, it is not surprising that the leakage observed is quite strong. The Raman line at $2\omega_{PM}$ has also been observed in right-angle scattering. As expected, the Stokes component appears in $(\hat{\sigma}_+,\hat{y})$ for the geometry shown in Fig. 1(a), while the anti-Stokes component is observed in the $(\hat{\sigma}_-,\hat{y})$ polarization. For the geometry of Fig. 1(b), the Stokes and anti-Stokes components are seen in the $(\hat{x},\hat{\sigma}_-)$ and the $(\hat{x},\hat{\sigma}_+)$ configurations, respectively.

It is known that electrons and holes in polar crystals interact strongly with zone-center longitudinal-optical (LO) phonons through the Fröhlich interaction.[21] A LO phonon can be created or annihilated as a result of such an interaction. Referring to the mechanism responsible for the ω_{PM} line, shown in Fig. 4, one can visualize a fourth step in which the excited electron or hole interacts with the lattice and creates or annihilates a LO phonon. Such a mechanism would result in a scattered photon with a Raman shift of $\omega_{LO}\pm\omega_{PM}$. The net result for the Stokes process with a shift of $\omega_{LO}+\omega_{PM}$ is that a LO phonon is created and a Mn^{2+} ion is excited to the next sublevel of the Zeeman multiplet. A Stokes shift of $\omega_{LO}-\omega_{PM}$ corresponds to the creation of a LO phonon and the deexcitation of a Mn^{2+} ion to the next lower sublevel of the multiplet. The $\omega_{LO}+\omega_{PM}$ Stokes-Raman line is expected to appear in the $(\hat{\sigma}_+,\hat{z})$ or the $(\hat{z},\hat{\sigma}_-)$ configurations, whereas the $\omega_{LO}-\omega_{PM}$ Stokes line is allowed for $(\hat{\sigma}_-,\hat{z})$ or $(\hat{z},\hat{\sigma}_+)$.

In addition to the above, the creation or annihilation of two LO phonons in a similar process is also possible. An electron or a hole can create or annihilate two LO phonons in a single step. Another possibility is that an electron as well as a hole each separately create a LO phonon. In either case, the scattered photon can have the following Raman shifts: $2\omega_{LO_1}\pm\omega_{PM}$, $\omega_{LO_1}+\omega_{LO_2}\pm\omega_{PM}$, or $2\omega_{LO_2}\pm\omega_{PM}$, where LO_1 refers to the CdTe-like and LO_2 the MnTe-like zone-center LO phonons.[8] As before, the Stokes lines involving the excitation of a Mn^{2+} ion are expected in the $(\hat{\sigma}_+,\hat{z})$ or $(\hat{z},\hat{\sigma}_-)$ polarization geometries, while those involving a deexcitation of a Mn^{2+} ion appear in $(\hat{\sigma}_-,\hat{z})$ or $(\hat{z},\hat{\sigma}_+)$.

The new lines described above should occur only under conditions of band-gap resonance. Under such conditions, we have indeed observed the new Raman lines with shifts of $\omega_{LO}\pm\omega_{PM}$ in $Cd_{1-x}Mn_xTe$ for a variety of compositions. The Raman spectra in the region of the longitudinal- and transverse-optical (TO) vibrational modes are shown in Fig. 7 for $Cd_{1-x}Mn_xTe$ with $x=0.10$. The 7525-Å Kr^+ laser line was used to excite the spectra; the scattering geometry is that of Fig. 1(b). The zero magnetic field LO and TO phonon spectrum is shown in Fig. 7(b). Here the CdTe-like TO and LO and the MnTe-like LO modes are quite distinct, while the MnTe-like TO appears as a shoulder to the LO (Ref. 8). The corresponding Raman spectra, recorded in the presence of a magnetic field of 60 kG and in the $(\hat{z},\hat{\sigma}_+)$ and $(\hat{z},\hat{\sigma}_-)$ configurations, are presented in Figs. 7(a) and 7(c), respectively. The additional Raman lines with Stokes shifts $\omega_{LO}\pm\omega_{PM}$ are clearly present with the proper polarization characteristics. The sample temperature was 120 K; at this temperature, the Mn^{2+}-ion Zeeman multiplet sublevel occupation probability ratio $\exp(-\hbar\omega_{PM}/k_BT)=0.94$. Thus the intensity of the $\omega_{LO}+\omega_{PM}$ line and that of $\omega_{LO}-\omega_{PM}$ are expected to be approximately equal. The $\omega_{LO}\pm\omega_{PM}$ lines can be observed only when the exciting photon energy is strongly resonant with the band gap. There is no evidence of corresponding Raman lines associated with the TO phonons, which would have shifts of $\omega_{TO}\pm\omega_{PM}$. This supports the assumption that the Fröhlich interaction is responsible for the appearance of the new features.

The portion of the Raman spectrum containing the combination mode $\omega_{LO_1}+\omega_{LO_2}$ and the overtones $2\omega_{LO_1}$ and $2\omega_{LO_2}$ is shown in Fig. 8 for $Cd_{1-x}Mn_xTe$ with $x=0.175$. The spectrum was recorded for $T=6$ K and $H=60$ kG in the backscattering geometry using $\lambda_L=6471$ Å as the exciting line; the crystal is opaque to this wavelength. The band gap coincides with the photon energy of the scattered radiation ("out resonance") as indicated by the rising background due to interband luminescence. In Fig. 8 the arrows indicate the new features with shifts of $2\omega_{LO_1}+\omega_{PM}$ and $\omega_{LO_1}+\omega_{LO_2}+\omega_{PM}$. For this small value of x, the $2\omega_{LO_2}$ line is weak[8] and, in addition, it is superimposed on the luminescence background, making the observation of the $2\omega_{LO_2}+\omega_{PM}$ line difficult. At this low temperature, processes involving the deexcitation of a Mn^{2+} ion are expected to have very low probability, explaining the absence of features with shifts $2\omega_{LO_1}-\omega_{PM}$, $\omega_{LO_1}+\omega_{LO_2}-\omega_{PM}$, and $2\omega_{LO_2}-\omega_{PM}$.

The Raman lines described above $(2\omega_{PM},\omega_{LO}\pm\omega_{PM},\ldots,)$ were observed only under resonant conditions involving the band gap. It is possible that the same lines will appear when the resonance is associated with the internal transitions of the Mn^{2+} ion. For example, the $2\omega_{PM}$ Raman line can occur with a mechanism similar to that in

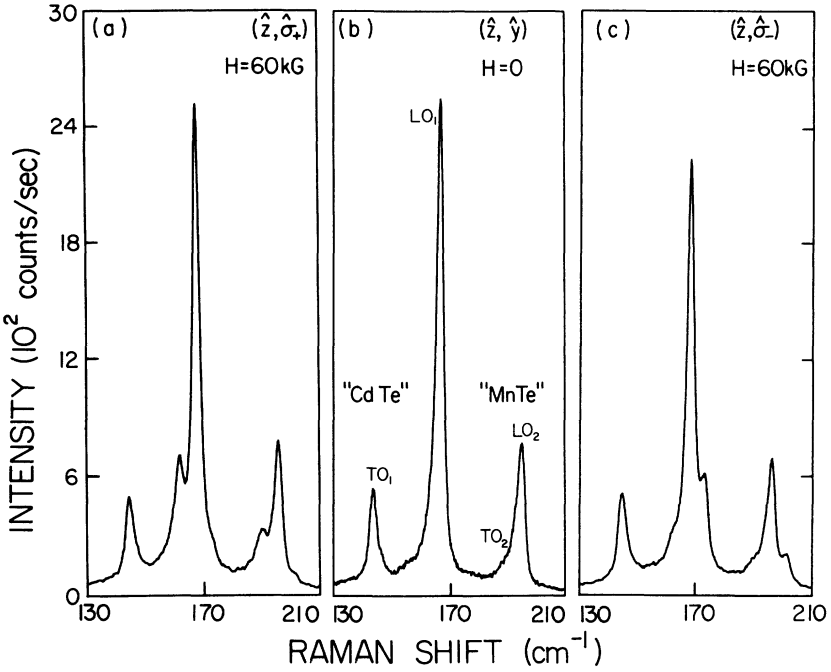

FIG. 7. Raman spectra of $Cd_{1-x}Mn_xTe$, $x=0.10$, showing the combination lines $\omega_{LO_1}\pm\omega_{PM}$ and $\omega_{LO_2}\pm\omega_{PM}$, where LO_1 and LO_2 are the CdTe-like and MnTe-like LO phonons. The scattering geometry used is shown in Fig. 1(b). The sample temperature $T=120$ K, $H=60$ kG, and $\lambda_L=7525$ Å; x, y, and z are along [110], [001], and [1$\bar{1}$0], respectively.

Fig. 3. For the Stokes component, a photon of polarization $\hat{\sigma}_+$ induces a virtual electric dipole transition between an initial and an intermediate state which differ by $\Delta m_J=+1$; it is followed by a second transition between the intermediate and final states with $\Delta m_J=-1$, and accompanied by the emission of a photon of polarization $\hat{\sigma}_-$. The polarization characteristics are thus the same as in the interband mechanism. We note that the same number of internal transitions are involved for both the ω_{PM} and $2\omega_{PM}$ Raman lines. It is also possible to visualize transitions similar to those in Fig. 3 in which an additional step involves a vibrational mode which could be either a local mode or a phonon. Clearly, these conjectures have to be tested close to the resonance Raman conditions associated with the internal transitions of Mn^{2+}.

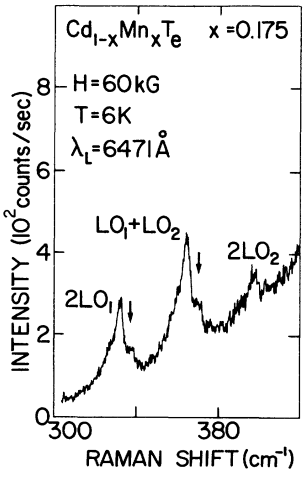

FIG. 8. Raman spectra of $Cd_{1-x}Mn_xTe$, $x=0.175$, showing the combination lines $2\omega_{LO_1}+\omega_{PM}$ and $\omega_{LO_1}+\omega_{LO_2}+\omega_{PM}$ indicated by arrows. A backscattering geometry was used, with (110) as the scattering face. The incident polarization was vertical (normal to the magnetic field) and the scattered light was unanalyzed.

B. Magnetically ordered phase

As mentioned in Sec. I, $Cd_{1-x}Mn_xTe$ exhibits a magnetically ordered low-temperature phase for $x>0.17$. The transition from the paramagnetic to the magnetically ordered phase is accompanied by the appearance of a new Raman feature at low temperatures.[7,8] Since this excitation is associated with magnetic order, it has been attributed to a magnon. A distinct magnon feature was observed in $Cd_{1-x}Mn_xTe$ for the composition range $0.40\leq x\leq 0.70$. We show this in Fig. 9 at $T=5$ K for $x=0.55$, 0.65, and 0.70 having Raman shifts of $\sim$8, 10, and 12 cm^{-1}, respectively. The magnon feature is absent when the incident and the scattered polarizations are parallel and appears when they are

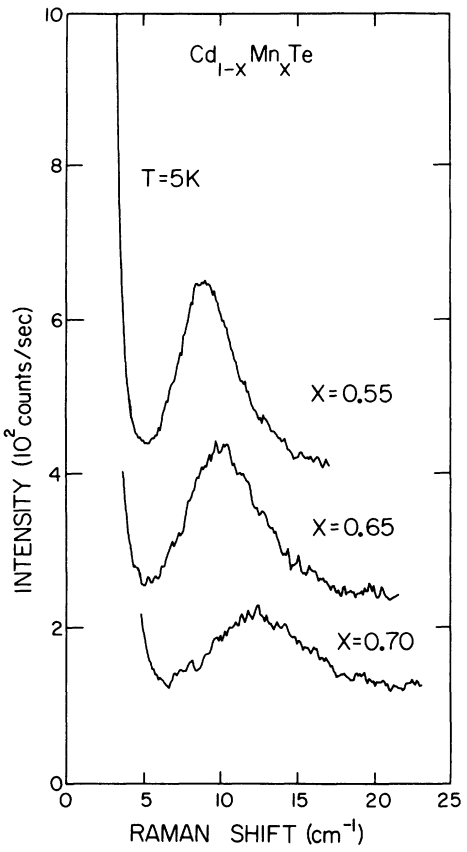

FIG. 9. Raman spectra of the zero-field magnon for $Cd_{1-x}Mn_xTe$ with $x=0.55$, 0.65, and 0.70. The spectra were excited using $\lambda_L=6764$ Å at $T=5$ K. The polarization is $(\hat{o}_+,\hat{z})$ and the geometry of Fig. 1(a) was used. The data for $x=0.55$ and 0.65 have been displaced vertically for clarity.

crossed. This was found to be the case for several crystallographic orientations as well as for polycrystalline samples. Such a behavior, irrespective of the crystallographic orientation, is exhibited only by an excitation whose Raman tensor is antisymmetric. As the temperature is increased, the Raman shift of the magnon ω_M decreases, and above a characteristic Néel temperature $T_N(x)$ the feature is no longer observable. For $x=0.70$, the temperature dependence of ω_M follows a Brillouin function.

The magnon feature described above occurs both in the spin-glass and the antiferromagnetic phase.[8] Its polarization characteristics as well as the temperature behavior are similar in both cases indicating no qualitative difference in the excitation whether observed in the spin-glass or the antiferromagnetic phase. Recent work[5,22,23] has indeed brought out the similarity between the two phases. Escorne and Mauger[22] were able to interpret their magnetic susceptibility data in $Cd_{1-x}Mn_xTe$ ($x\leq 0.50$) on the basis of an antiferromagnetic clustering model rather than that of a spin-glass. Neutron scattering experiments[5] performed on $Cd_{1-x}Mn_xTe$ for $0.60\leq x\leq 0.70$ indicate that there is no long-range magnetic ordering at low temperatures even for this composition range; instead, the Mn^{2+} ions form antiferromagnetically ordered spin clusters. In the light of these observations it appears that the spin-glass ($0.17\leq x\leq 0.60$) and the antiferromagnetic phase ($0.60\leq x\leq 0.70$) are physically similar, with the average size of the spin clusters increasing with x.

As can be seen in Fig. 9, the magnon features are rather broad and asymmetric. The width increases with increasing x. From the theoretical calculations of Ching and Huber[23] based on a cluster model for a dilute array, such a broadening with x can be expected. We now proceed to discuss the implication of the cluster model for interpreting our data. In $Cd_{1-x}Mn_xTe$ a given Mn^{2+} ion in the lattice may have up to twelve Mn^{2+} ions as nearest neighbors (NN), arranged in a type-III antiferromagnetically ordered face-centered-cubic (fcc) lattice.[5] Eight of these NN sites may be occupied by ions with their spins aligned antiparallel to that of the Mn^{2+} ion under consideration, while the remaining four NN sites may have ions with their spins aligned parallel. Manganese ions would be present at all twelve NN sites for $x=1$, i.e., for a hypothetical cubic MnTe crystal.

The Heisenberg Hamiltonian for the antiferromagnetic exchange coupling of the Mn^{2+} ions is given by

$$H=\sum_{m,n}{}'J(\vec{R}_m-\vec{R}_n)\vec{S}_m\cdot\vec{S}_n=\sum_{m,n}{}'J_{mn}\vec{S}_m\cdot\vec{S}_n\ , \tag{5}$$

where J_{mn} is the exchange integral, $\vec{R}_n$ is the position, and $\vec{S}_n$ is the spin operator for a Mn^{2+} ion. For the zinc-blende structure the exchange constant for next-nearest neighbors (NNN), $J_{\rm NNN}$, may be neglected[3,24] in comparison with the exchange constant for nearest neighbors, J_{NN}. Hence the sum of Eq. (5) may be limited to nearest neighbors only.

Using molecular-field theory, one can write a single-ion Hamiltonian[25]

$$H_n=2J\vec{S}_n\cdot\sum_m\vec{S}_m\ , \tag{6}$$

where $J=J_{\rm NN}$ and the summation extends only over the manganese ions in the NN sites. From Eq. (6) the exchange field $\vec{H}_E$ is given by

$$\vec{H}_E=-\frac{2ZJ\langle\vec{S}\rangle}{g\mu_B}\ , \tag{7}$$

where $\langle\vec{S}\rangle$ is the thermal average of the Mn^{2+}-ion spin, and $Z=Z_a-Z_p$ is the difference between the number of NN ions with their spins aligned antiparallel to that of the ion in question, Z_a, and the number aligned parallel, Z_p. As is shown in Eq. (7), the exchange field is proportional to Z; hence any local variation in Z will result in a corresponding variation in H_E. (See also Ref. 23.) The magnon energy $\hbar\omega_M$ is expected to increase with H_E. Since the distribution of Mn^{2+} ions in $Cd_{1-x}Mn_xTe$ is random, one expects a local variation of Mn^{2+} concentration, with the corresponding variation in Z and H_E, which in turn will result in a distribution of magnon frequencies, rather than a sharp feature. As seen in Fig. 9, this is indeed the case; the width of the magnon feature increases with x, due to the increase in the number of probable values of Z. (See Ref. 23.) For higher values of x a more significant number of the ions will have the full or close to the full complement of nearest neighbors. These ions would constitute the cores of the antiferromagnetically ordered spin clusters. Hence the magnon feature may be viewed as the spin excitation of the Mn^{2+} ions in the presence of a distribution of exchange fields derived from a distribution of Z.

The magnon feature in the presence of an external magnetic field of 60 kG is shown in Figs. 10(a) and 10(c) for $Cd_{1-x}Mn_xTe$, $x=0.70$. The spectrum shown in Fig. 10(a) was recorded at $T=5$ K with $\lambda_L=5682$ Å in the $(\hat{\sigma}_-,\hat{z})$ polarization while the spectrum in Fig. 10(c) was observed in the $(\hat{\sigma}_+,\hat{z})$ configuration. In the following we discuss the Stokes components of these Raman features. The Raman shifts of the peaks of the features in Fig. 10 are $\omega_{M_-}=8.5$ cm^{-1}, $\omega_M=12$ cm^{-1}, and $\omega_{M_+}=15.5$ cm^{-1}. It can be shown[17] that a one-magnon Raman line in an antiferromagnet should split into two components of equal intensity separated by $2g\mu_BH$ at $T=0$ K, if $\vec{H}$ is along the anisotropy field $\vec{H}_A$. The observed spacing between M_+ and M_- of 7 cm^{-1} for 60 kG is significantly smaller than $2g\mu_BH=11$ cm^{-1}. The polarization characteristics of ω_{M_+} and ω_{M_-} are those expected. These results are independent of the crystal orientations with respect to the applied field suggesting that H_A is small compared to the applied field. In Ref. 8, H_E for $x=0.7$ was calculated from the observed transition temperature $T_N=40$ K to be 208 kG, while H_A was determined to be $\sim$36 kG as deduced from $\hbar\omega_M=g\mu_B(H_A^2+2H_AH_E)^{1/2}$, strictly applicable to an antiferromagnet exhibiting long-range order. While the value for H_E is reasonable, that for H_A must be viewed as too large in the context of the present experimental results.

In the presence of an external magnetic field, the total magnetic field an ion will experience is $\vec{H}_E+\vec{H}$. In our experiments, $H_E>H$ for low temperatures[8]; the crystalline anisotropy field is assumed to be negligible in view of our observation that the magnetic field splitting of the magnon is independent of the direction of the applied field. This allows the Mn^{2+} ions to be oriented with their spins either parallel ($m_S=+\frac{5}{2}$) or antiparallel ($m_S=-\frac{5}{2}$) to the applied magnetic field. In the $(\hat{\sigma}_+,\hat{z})$ configuration, the M_+ Stokes component corresponds to the excitation of Mn^{2+} ions with $m_S=-\frac{5}{2}$ (magnetic moment $\vec{\mu}$ parallel to $\vec{H}$), while the M_- anti-Stokes component is associated with the deexcitation of ions with their magnetic mo-

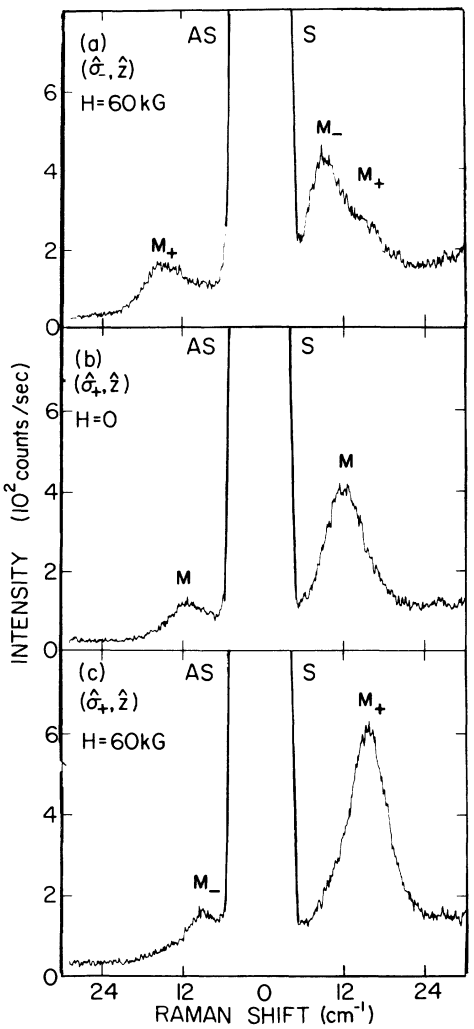

FIG. 10. Effect of the magnetic field on the magnon feature of $Cd_{1-x}Mn_xTe$, $x=0.70$, at $T=5$ K with $\lambda_L=5682$ Å. The geometry used is that of Fig. 1(a); x, y, and z are along [110], [$\bar{1}$10], and [001], respectively. Owing to imperfect polarization results, leakage of the fairly strong feature M_+ appears as a small shoulder in the $(\hat{\sigma}_-,\hat{z})$ configuration.

ments antiparallel to $\vec{H}$. The reverse is the case for features with $(\hat{\sigma}_-,\hat{z})$ polarization characteristics; the M_- Stokes component results from the excitation of Mn^{2+} ions with $m_S=+\frac{5}{2}$ ($\vec{\mu}$ is antiparallel to $\vec{H}$), while the M_+ anti-Stokes feature corresponds to the deexcitation of ions with $\vec{\mu}$ parallel to $\vec{H}$. We note that the feature M_+ in Fig. 10(c) is broader and more intense than either M or M_-. This may be due to the distortion of the magnetic structure of the clusters caused by the application of an external magnetic field, which is a significant fraction of the exchange field experienced by the Mn^{2+} ions.

We have described the Raman features associated with magnetic excitations appearing in the paramagnetic state as well as in the magnetically ordered phase. The exchange interaction between Mn^{2+} ions is negligible compared to k_BT at high temperatures becoming more important as the temperature is lowered. It is of interest to investigate the effects of temperature on the ω_{PM} line, particularly the effect of lowering the temperature below T_N, the transition temperature characterizing the magnetically ordered phase. The temperature evolution of the ω_{PM} line is shown for $Cd_{1-x}Mn_xTe$, $x=0.70$, in Fig. 11. The spectra were recorded for a magnetic field of 60 kG using the $(\hat{\sigma}_+,\hat{z})$ configuration. As the temperature is lowered, the ω_{PM} line initially broadens and then moves towards higher Raman shifts as a consequence of the increased importance of the exchange interaction. An increase in Raman shift is observed at temperatures well above $T_N\sim40$ K. As the temperature is lowered through and below T_N, the line becomes the magnon component observed in the $(\hat{\sigma}_+,\hat{z})$ configuration.

IV. CONCLUDING REMARKS

This paper illustrates the versatility of Raman spectroscopy in investigating a wide range of excitations. In its application to the diluted magnetic semiconductors, it has enabled the observation of a variety of magnetic excitations. The mechanisms underlying the Raman scattering associated with the paramagnetic transitions within the Zeeman multiplet—the ω_{PM} Raman line—can provide microscopic insights into the internal levels of Mn^{2+}, the exchange interaction between band electrons and Mn^{2+}, and that between Mn^{2+} ions among themselves. It is the Mn^{2+}-Mn^{2+} interaction which results in the magnetic phase exhibited by the diluted magnetic semiconductors. The ability to follow the evolution of the ω_{PM} line into the magnon feature as the temperature is lowered through the Néel temperature is particularly useful in providing an insight into the nature of the magnetic phase. In this context we note that the EPR work of Oseroff *et al.*[14] and Oseroff[15] on $Cd_{1-x}Mn_xTe$ and $Cd_{1-x}Mn_xSe$ is limited to the paramagnetic phase for large values of x; it is precisely in this context that Raman scattering is effective.

Although the data reported here are for $Cd_{1-x}Mn_xTe$, the other diluted magnetic semiconductors should show similar Raman spectra. Indeed, we have seen some of the excitations report-

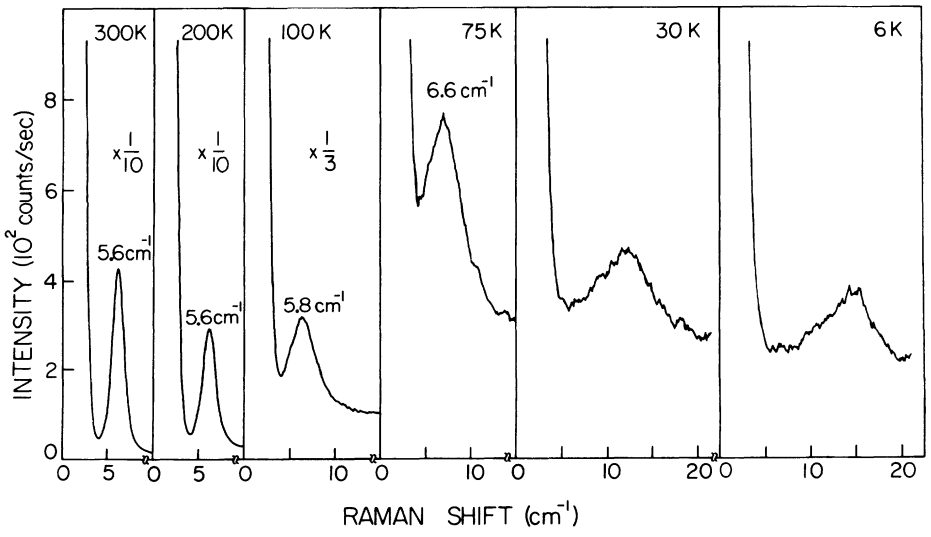

FIG. 11. Evolution of the Raman line at ω_{PM} of $Cd_{1-x}Mn_xTe$, $x=0.70$, into the magnon feature as the temperature is lowered from room temperature to below the Néel temperature. The spectra were recorded with $H=60$ kG, $\lambda_L=6764$ Å in the $(\hat{\sigma}_+,\hat{z})$ polarization using the geometry of Fig. 1(a); x, y, and z are along [110], [$\bar{1}$10], and [001], respectively.

ed here in $Zn_{1-x}Mn_xTe$, $Cd_{1-x}Mn_xSe$, and $Cd_{1-x}Mn_xS$. The ω_{PM} line has also been observed in $Cd_{1-x}Mn_xS$ and $Zn_{1-x}Mn_xSe$ by Douglas *et al.*[26] The Raman scattering data for diluted magnetic semiconductors that we have presented and discussed in this paper are associated with the spin flip of the $3d$ electrons localized in the Mn^{2+} ions. It should be contrasted with the Raman scattering associated with the spin flip of free electrons or electrons bound to donors in large effective-mass orbits, as first reported by Geyer and Fan[27] in $Hg_{1-x}Mn_xTe$, later by Nawrocki *et al.*[28] in $Cd_{1-x}Mn_xSe$, and by Peterson *et al.*[29] in $Cd_{1-x}Mn_xTe$.

Finally, the conclusion that the magnetic feature observed in the magnetically ordered phases is a one-magnon excitation was initially deduced from its polarization characteristics and temperature behavior[7,8]; this is supported by the results of Ching and Huber.[23] The fact that this feature shows a splitting in the presence of a magnetic field and that the ω_{PM} line of the paramagnetic phase, clearly associated with a single-ion excitation, evolves smoothly into the higher-energy component of the magnon, provides a strong confirmation of this interpretation. In the same spirit, one might expect a two-magnon feature associated with the $2\omega_{PM}$ line; however, given the intensity of the $2\omega_{PM}$ line compared to that of the ω_{PM} line, the intensity of such a feature would preclude its observation. A two-magnon feature similar to that seen in MnF_2 by Fleury and Loudon[17] would have symmetric polarization characteristics; such a feature has also not been observed in $Cd_{1-x}Mn_xTe$. In the light of these experimental results, the two-magnon interpretation advanced by Grynberg and Picquart[30] to explain the feature at ω_M is clearly excluded.

ACKNOWLEDGMENTS

We wish to thank J. K. Furdyna, R. L. Aggarwal, and M. Dutta for stimulating discussions. We express our appreciation to W. Giriat and D. C. Reynolds for providing some of the samples used in this investigation. This work was supported in part by National Science Foundation Grant No. DMR-81-06144 and National Science Foundation—Materials Research Laboratory Program No. DMR-80-20249. A. P. thanks the Purdue Research Foundation for a David Ross Fellowship. D. L. P. expresses his appreciation to the Eastman Kodak Company for a Kodak Fellowship.

---

*Present address: Department of Physics, State University of New York, Binghamton, NY 13901.

†Present address: Institute of Physics, Polish Academy of Sciences, Warsaw, Poland.

[1]J. K. Furdyna, J. Appl. Phys. 53, 7637 (1982).

[2]R. R. Galazka, in *Proceedings of the 14th International Conference on the Physics of Semiconductors, Edinburgh, 1978,* edited by B. L. H. Wilson (IOP, Bristol, 1978), p. 133.

[3]R. R. Galazka, S. Nagata, and P. H. Keesom, Phys. Rev. B 22, 3344 (1980).

[4]S. Nagata, R. R. Galazka, D. P. Mullin, H. Akbarzadeh, G. D. Khattak, J. K. Furdyna, and P. H. Keesom, Phys. Rev. B 22, 3331 (1980); G. D. Khattak, C. D. Amarasekara, S. Nagata, R. R. Galazka, and P. H. Keesom, *ibid.* 23, 3553 (1981).

[5]T. Giebultowicz, H. Kepa, B. Buras, K. Clausen, and R. R. Galazka, Solid State Commun. 40, 499 (1981).

[6]T. M. Holden, G. Dolling, V. F. Sears, J. K. Furdyna, and W. Giriat, Solid State Commun. 40, 281 (1981).

[7]S. Venugopalan, A. Petrou, R. R. Galazka, and A. K. Ramdas, Solid State Commun. 38, 365 (1981).

[8]S. Venugopalan, A. Petrou, R. R. Galazka, A. K. Ramdas, and S. Rodriguez, Phys. Rev. B 25, 2681 (1982).

[9]Short reports have been presented in the following: A. K. Ramdas and S. Rodriguez, in *Novel Materials and Techniques in Condensed Matter,* edited by G. W. Crabtree and P. Vashishta (North-Holland, New York, 1982), p. 209; A. Petrou, D. L. Peterson, S. Venugopalan, R. R. Galazka, A. K. Ramdas, and S. Rodriguez, Bull. Am. Phys. Soc. 27, 336 (1982); Phys. Rev. Lett. 48, 1036 (1982).

[10]Special "SuperVaritemp" Optical Magnet Cryostat with $6T$ S/C Magnet, Janis Research Co., 22 Spencer St., Stoneham, MA 02180.

[11]Model DTC-500 SP Cryogenic Temperature Indicator/Controller, Lake Shore Cryotronics, Inc., 64 East Walnut St. Westerville, OH 43081.

[12]A. Abragam and B. Bleaney, *Electron Paramagnetic Resonance of Transition Ions* (Clarendon, Oxford, 1970), p. 143.

[13]J. Lambe and C. Kikuchi, Phys. Rev. 119, 1256 (1960).

[14]S. B. Oseroff, R. Calvo, W. Giriat, and Z. Fisk, Solid State Commun. 35, 539 (1980).

[15]S. B. Oseroff, Phys. Rev. B 25, 6584 (1982).

[16]S. Al'tshuler, Y. Nazarov, and A. K. Khasanov, Pis'ma Zh. Eksp. Teor. Fiz. 33, 525 (1981) [JETP Lett. 33, 508 (1981)].

[17]P. A. Fleury and R. Loudon, Phys. Rev. 166, 154 (1968).

[18]R. Loudon, J. Raman Spectrosc. 7, 10 (1978).

[19]N. T. Khoi and J. A. Gaj, Phys. Status Solidi B 83, K133 (1977).

[20]J. A. Gaj, J. Ginter, and R. R. Galazka, Phys. Status Solidi B 89, 655 (1978).

[21]W. Hayes and R. Loudon, *Scattering of Light by Crys-*

tals (Wiley, New York, 1978), pp. 179–183.
[22]M. Escorne and A. Mauger, Phys. Rev. B 25, 4674 (1982).
[23]W. Y. Ching and D. L. Huber, Phys. Rev. B 25, 5761 (1982); 26, 6164 (1982).
[24]W. H. Brumage, C. R. Yarger, and C. C. Lin, Phys. Rev 133, A765 (1964).
[25]J. Callaway, *Quantum Theory of the Solid State* (Academic, New York, 1974), p. 88.
[26]K. Douglas, S. Nakashima, and J. F. Scott, Bull. Am. Phys. Soc. 27, 13 (1982).
[27]F. F. Geyer and H. Y. Fan, IEEE J. Quant. Electron QE-16, 1365 (1980).
[28]M. Nawrocki, R. Planel, G. Fishman, and R. R. Galazka, Phys. Rev. Lett. 46, 735 (1981).
[29]D. L. Peterson, A. Petrou, M. Dutta, A. K. Ramdas, and S. Rodriguez, Solid State Commun. 43, 667 (1982).
[30]M. Grynberg and M. Picquart, J. Phys. C 14, 4677 (1981).